IAM2022-91705

DEVELOPMENT OF A NEW MANUFACTURING ROUTE BY DIRECT LASER METAL DEPOSITION WITH NiCrSiFeB ALLOYS TO REPLACE COBALT IN AERONAUTICAL COMPONENTS

Juan Carlos Pereira[1], Fidel Zubiri[1], David Aguilar[1], Maria Del Carmen Taboada[1], Gaylord Guillonneau[2], Jerome Rocchi[3]

[1]LORTEK Technological Centre, Basque Research and Technology Alliance BRTA, Gipuzkoa, Spain
[2]Ecole Centrale de Lyon - Laboratoire de Tribologie et Dynamique des Systèmes, Toulouse, France
[3]LIEBHERR Aerospace Toulouse SAS, Toulouse, France

ABSTRACT

Nickel-based NiCrSiFeB alloy (Ni-Cr-Si-B self-fluxing family) are excellent candidates for replacing Cobalt-based alloys in aeronautical components such as sealing rings, valve seats, sliding bearing seats, etc. In this type of components, commonly manufactured by centrifugal casting and conventional processes, high temperature wear and stiffness under complex thermo-mechanical stresses cause lack of sealing and an increase in the wear rate. Metal additive manufacturing by direct laser metal deposition with powder (p-LMD) is presented as a potential manufacturing route for the complex processing of this type of alloys. This research work deals with the development of a new manufacturing route using p-LMD that ranges from the proper selection of the chemical composition for the starting powders, the development of the LMD process parameters to tackle the challenges associated to the wide solidification range and crack susceptibility of Ni-Cr-Si-B alloys, its monitoring and control, as well as the post-processing required to achieve the manufacture of aeronautical components. In this work, the porosity analysis, as-built microstructure, hardness at room temperature and at high temperature, and the strengthening mechanisms have been studied in cylinders manufactured with different chemical composition grades and LMD process parameter sets (slow, normal and fast deposition speed).

Keywords: additive manufacturing; directed energy deposition; laser metal deposition; self-fluxing alloys; NiCrSiB; sealing rings.

1. INTRODUCTION

Self-fluxing alloys consists of Nickel and Cobalt based materials with a proven record of accomplishment for hardfacing applications[1]. In this research work, the focus is on Nickel-based Self-fluxing alloys, and in particular, the NiCrSiFeB alloy variant is of the interest to substitute current Co-based alloy used in aeronautic components, like in sealing rings, valve seats, sliding bearing seats, etc. New Nickel based self-fluxing alloys offering high hardness (up to 60 HRC) are available on powder format only, mainly used to obtain coatings by means of thermal spray or arc processes such as High Velocity Oxy Fuel (HVOF) and Plasma Transferred Arc (PTA)[2]. NiCrSiFeB alloys are developed and commonly used for coatings in different applications in which resistance to wear, corrosion and heat is required, such as in boilers of coal fueled power plants or gas turbines, depending on working conditions that generates a specific wear type. The type and severity of wear depends on many interacting factors including applied load, relative movement and temperature. Wear may be less severe at high temperature than at low temperatures in some cases, because of the beneficial effects of oxides, particularly Cobalt and Iron oxides that modify wear kinetics, but is not a general rule. Poor oxide adherence, however, could result in accelerated wear.

Ni-Cr-B-Si alloys are among the most widely used hardfacing alloys for wear and corrosion protection[1]. Common deposition techniques include thermal spraying, fuse techniques and laser cladding[1], [3]. However, there is almost no information about the properties and microstructures of these alloys in casting applications, since these alloys mainly used for coatings. However, an application of Ni-based self-fluxing materials is the fabrication of wear resistant cylinder linings by centrifugal casting (US Patent 4.427.446) and in sealing rings.

Hemmati *et al*[4], [5] observed that there is a strong relation between alloy composition and phase formation, microstructure and properties in laser clad Ni-Cr-B-Si deposits. They stated that phase formation of Ni-Cr-B-Si laser deposited coatings primarily depends on the Cr content and Si/B ratio with the former controlling the amount of Cr-rich precipitates and the latter influencing the nature of the eutectic structures. The high-alloy grades revealed numerous Cr boride precipitates, a low Si/B ratio

(Si/B = 1.5) and substantial Ni-B-Si eutectics, while the low-alloy grades showed very little Cr boride precipitates, a high Si/B ratio (Si/B > 3) and small amounts of interdendritic eutectics. The high amounts of hard Cr-rich precipitates and the eutectic structures produced high hardness levels. The effect of lower Cr content and higher Si/B ratio was to reduce the quantity of borides and modifying the nature of the eutectic phases. Similar tendencies can be expected to occur in the centrifugal cast structures.

In the case of Cobalt superalloys, the hardness and wear resistance of these alloys are increased with the carbide volume and also is critical carbides composition and morphology[6]. Nickel superalloys have a high variety of strengthening mechanisms: solid solution strengthening, Laves phases formation, precipitation hardening and dispersion strengthening, whose combination can empower wear and high temperature properties. This research work will help to improve cabin air quality by avoiding potential wear particles of cobalt alloys, but also the need of higher wear resistant sealing rings, leakage-free valve in new hotter, and more pressurized bleed air for the future engines and the future less bleed Environmental Control Systems (ECS). This research work is supported by Clean Sky JTI (Joint Technology Initiative) and Liebherr -Aerospace Toulouse SAS as topic manager.

According to ISO/ASTM 52900 standard[7], Directed Energy Deposition (DED) is the AM process that uses a focused thermal energy source (laser, electron beam or plasma arc) to fuse materials as they are deposited. DED technology covers multiple direct metal deposition processes according to the thermal source used, such as Laser Metal Deposition -LMD, Wire and Arc Additive Manufacturing -WAAM and Electron Beam Additive Manufacturing -EBAM. Among these processes, powder-LMD process that utilizes a laser beam to melt the powder delivered coaxial to the beam has been chosen for this work. LMD is a key process for improved design and manufacturing of near-net-shape parts. In fact, some recent progress are published recently by some authors[8], [9]. This process allows obtaining lower layer height and better resolution and accuracy compared with WAAM, and lower investment and implementation cost compared with EBAM. Moreover, WAAM and EBAM has the following drawbacks: limited availability of commercial wire materials and they are more difficult processes to control. Besides, it is worth to mention that LMD allows changing the design (size, material, and shape) of the part/component easily without major impacts on the manufacturing process chain, reducing time-to-market.

Among the expected benefits of using LMD as industrial alternative, is to achieve a flexible manufacturing route, which allows reducing design, manufacturing, and market entry times, with less environmental impact than current manufacturing solutions like centrifugal casting, gravity casting, and to reach similar or superior high temperature wear behavior (up to 700 °C) of the Stellite 6 alloy currently used for aeronautical components.

The aim of this work is to select the most promising solution after evaluating three commercial composition grades of self-fluxing nickel alloys as starting point for a deep manufacturing processes study, and to obtain the optimum LMD process parameters set and deposition conditions for the additive manufacturing of preforms. The conclusions were stated after the evaluation of as-built microstructure and hardness based on the measurement of hot hardness and electron microscopy analysis in cylindrical samples manufactured by LMD. The comparative of hardness behaviour at room temperature and at high temperature with Stellite 6, as reference material used on the current manufacturing route of the aeronautical parts targeted, were made.

2. MATERIALS AND METHODS

In this section are stated all materials, equipment and methods that have been used in the research work. We start with the selection of three potential composition grades from commercial Ni-Cr-Si-B alloys powders, and then we manufactured a bar of the reference material (Stellite 6) used in the comparative analysis. Afterwards we explained the LMD set-up used for the manufacturing of test samples.

2.1 NiCrSiFeB alloys

In this research work, three Nickel-based self-fluxing alloys as raw materials were selected due their potential to promote the glaze layer formation during wear at HT (certain Fe content is needed), their content of Cr and C (as Carbides promoters), Borides promoters (B,Ni,Si,Cr), their corrosion resistance (Cr,Ni), and achievable hardness in as-built condition.

The gas atomized NiCrSiFeB powder particles were manufactured by Oerlikon Metco AG (Alloy A) and by Flame Spray Technologies B.V. (Alloys B and C), they were sieved to achieve a particle size of +53–125 μm in Alloy A, and +20–53 μm in Alloys B and C according to the technical specifications provided. The plates used as substrate (10 mm thickness) were manufactured with austenitic stainless steel (EN 1.4404) and was provided in a soft condition (hot-rolled and annealed). The chemical compositions reported by the manufacturers of the powders are showed in Table 1.

Table 1. Chemical composition of the preselected NiCrSiFeB alloys reported by powder manufacturers.

Alloy	Chemical composition (wt.%)						
	Ni	Cr	Si	Fe	B	C	Si/B
A	84.59	7.52	3.42	2.53	1.70	0.24	2.01
B	83.74	8.15	3.27	2.77	1.61	0.38	2.03
C	76.80	12.51	3.73	4.04	2.42	0.45	1.54

The pre-alloyed powders were analyzed in LORTEK using a field emission scanning electron microscope (FESEM) brand Zeiss Ultra Plus model, equipped with an X-ray detector from Oxford instruments (X-Max), which allowed not only to capture high resolution images of the particles, but also semi-quantitative chemical analysis using the energy dispersion spectroscopy (EDS) technique. The particles showed a spherical shape, a morphology commonly obtained from the gas atomization

procedure in their manufacturing. After the image analysis of the particles, the results revealed that the size of the 10% in volume of the particles presented less than 76.21, 33.52 and 33.06 microns in diameter for powders A, B and C respectively; 50% of the particles less than 94.80, 47.05, 47.19 microns; and a cumulative 90% volume of the powder particles had a diameter less than 116.05, 58.52 and 52.18 microns in each powder. The analysis of particle shape and size distribution (diameter) in the powder, is very important for the LMD process, for the adequate powder stream when using discrete coaxial nozzles. The particle size distribution of these particles is almost normal. Due to the typical powder feeder system used in DED process, a fine-medium granulometry and regular sizes and shapes are required, so an adequate flowability of the powder determines the optimal powder stream and efficiency in the coaxial nozzle for laser melting and deposition of the raw material in the AM process.

2.1 Stellite 6 reference material

The Cobalt-based alloy used in the aeronautic component part objective is called Stellite 6, whose chemical composition range is shown in table 2. This is the reference material for the study. The service provider of Liebherr -Aerospace Toulouse SAS manufactured a bar of D25 mm and 300 mm in length using the horizontal centrifugal casting process homologated by them.

Table 2. Chemical composition range of Stellite 6 (reference material).

	Chemical composition (wt.%)										
	C	Mn	Si	P	S	Cr	W	Ni	Mo	Fe	Co
Min	0.9	-	-	-	-	27	4	-	-	-	bal
Max	1.4	1.0	1.5	0.04	0.04	32	5.5	2.5	1	2.5	

2.3 Laser Metal Deposition equipment and set-up

The system used for the LMD process was a 4-axis Cartesian kinematic station equipped with classical CNC (FAGOR 8070, Spain), see Figure 1 (left), and a solid state 3 kW Nd:YAG laser source (Trumpf HL-3006D, Germany) operated in CW mode with a wavelength of 1064 nm, optic fiber of 600 µm, and a spot diameter of 2.2 mm. The configuration of the LMD station includes an optic head (Trumpf BEO D70B, Germany) with two on-axis camera/sensor ports, and an electric induction heating system (up to 1000 °C and 10 kW) with temperature control, installed in the CNC table. An induction preheating system and floating clamps was added. For powder delivery, the LMD station has a powder feeder with two 5 L heated hoppers (Oerlikon Twin 150, Switzerland) and a 3-jet discrete nozzle (3-Jet-SO16-F manufactured by FhG ILT, Germany), (Figure 1 right). Argon (10 L/min) was used as protective gas and as carrier gas (4 L/min flow at 2 bar).

In order to simplify the design of experiments (DoE) matrix, some process parameters were set as constants in the process development phase. A constant laser power of 700 W was used, and the tracks overlap was 37.5%. While the key process parameters to be modified in the DoE influences the laser energy density delivered, the solidification conditions of the molten metal, and to ensure a fixed layer thickness. The deposition

speed was varied in three levels: 1-slow, 2-medium, and 3-fast, using 300, 500 and 700 mm/min. The powder mas flow was adjusted for each speed to achieve a layer thickness of 0.7 mm. The three process parameters set and three composition grades for NiCrSiFeB alloys used derived in nine different experiments for the DoE.
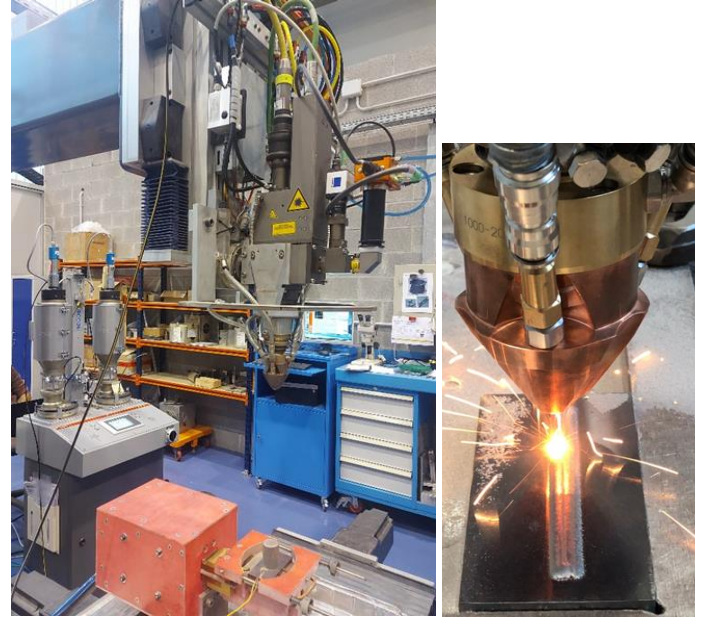

FIGURE 1: LMD-powder Cartesian station in LORTEK (left) and detail of 3-jet nozzle used (right)

2.4 Microstructural characterization and testing techniques

For microstructural evaluation, the cylinders were cut from the build plate and their cross section used for porosity and microstructure analysis. For hot hardness samples, the cylinders were machined to a lower diameter and additional disks (D25 and 5 mm in height) were extracted. Over these samples the metallographic preparations were made. The metallographic preparation procedure followed the guidelines of ASTM E3 standard. Beginning with the setting of the samples in conductive resin, then roughing them with abrasive papers of different grit sizes and ending with a fine polishing using polycrystalline diamond particles in an aqueous suspension. To reveal the microstructure, a chemical etch was carried out, using a chemical reagent recommended for this type of materials according to the ASTM E407 standard. The macro and microstructural analysis was carried out using a light optical microscopy (LOM) at different magnifications (from 100X to 1000X) with an Olympus GX51 optical microscope with an image acquisition system via digital camera. The chemical etching was carried out manually for 12 seconds with a reagent composed of 7 mL HF, 3 mL HNO3 and 5 mL of H2O. For more advanced studies in the microstructure, a FESEM was used also.

Microhardness Vickers measurements at room and a high temperature (650 °C) were made in a modified Buehler MacroMet 5112 durometer, using a load of 500 g (HV0.5 scale).

For the hot hardness measurements, the Vickers hardness device was modified to operate at elevated temperatures and incorporates a WC Vickers tip. The samples were heated at 650 °C and then cooled with a water-cooling device on each measurement. A thermal shield was installed on the mechanical components of the tester to avoid affectation. For temperature control, a K-type thermocouple was installed inside the samples using the lateral drill generated by electric discharge machining (EDM) in the discs. Five tests or indentations were made on one flat side of the disc, and then the hardness was obtained by measuring the diagonals of the indentations by interferometry, The high temperature hardness values were corrected for thermal expansion of the footprint. The Vickers hardness values were converted to Rockwell C hardness (HRC) for comparison purposes using the tables of ASTM E140-12B standard.

3. RESULTS AND DISCUSSION

The deposition strategy was optimized to obtain cylindrical specimens of diameter D32.5 mm and 35.2 mm in height with minimal geometrical distortions (near-net-shape). After the evaluation of material densification, macro/micro analysis of the material deposited in small volumes (4 layers), and the stability of the cylindrical geometry (verticality), a mixed deposition strategy was selected, combining a continuous bidirectional track for the hatch and a crossing pattern at 90° (each 2 layers). Also, the start/end points for the deposition of the contour track were alternated each 45°, and changed the direction of deposition in the contour track on every layer. Finally, double contour deposition every two layers were needed to ensure the stability of the cylinder contour and therefore, nearly perfect vertical cylinders were obtained replicating this 4-layer strategy for the rest of the build-up in the cylinder, as many as height desired in the cylinders.

In the process development of the cylinders preform, adequate material was obtained, also lower internal porosity and adequate layer thickness was achieved, but in alloys B and C. Some cracks appear at medium and high-speed deposition rates without a certain level of pre-heat of the build platform. To tackle this situation, in the last trials, it was decided to pre-heat the build plate at 400 °C and 500 °C for alloy B and C respectively, controlling the temperature of the build plate during the deposition and to make some slight tuning on the mass powder flow to achieve a layer thickness of 0.7 mm. Cross-sections of solid samples with 4 layers deposited were evaluated, and no significant cracks and other defects were observed. Then cylinders with 35.2 mm in height were produced for the three composition grades for testing and evaluation (see Figure 2). Nondestructive inspections were made (Visual and Penetrant tests), with positive results at least in the surface of the samples.

The first stage in the characterization of the samples was the measurement of internal porosity level in the nine cylinders. This was done evaluating the cross-section (XZ plane) of the cylinders with a metallographic preparation procedure followed by an image analysis of the micrographs taken with a digital camera system installed in the Light Optical Microscope (LOM) and using algorithms for the detection and classification of the porosities in terms of size and shape, and subsequent quantification in terms of porosity area (%) on each image. Six optical micrographs at 100X magnification were taken in different zones of each sample in study, to calculate then the mean value.
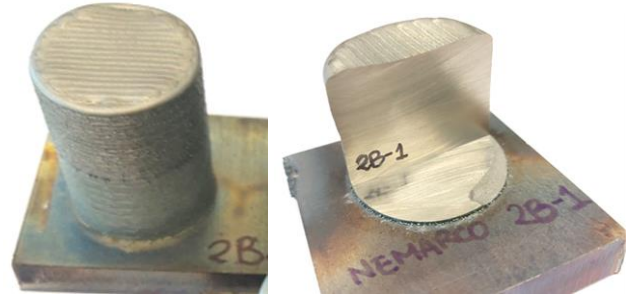

FIGURE 2: Example of one LMD cylinder sample 2B (left) and detail of sample cuts to evaluate their cross-section by microscopy examination (right)

Between the three compositions grades pre-selected, in the alloy A, a greater quantity of internal porosities in some particles was found than in the rest of the characterized powders. In the micrographs of Figure 3 we can see, as example, the porosity shape and distribution in the cross section of powder particles and then in the plane XZ of cylinders obtained by LMD. The worst results were obtained with alloy A independently of the LMD process parameters used, and the best results were achieved in general with the Alloy C, with the higher densification obtained using fast deposition speed (sample 3C).
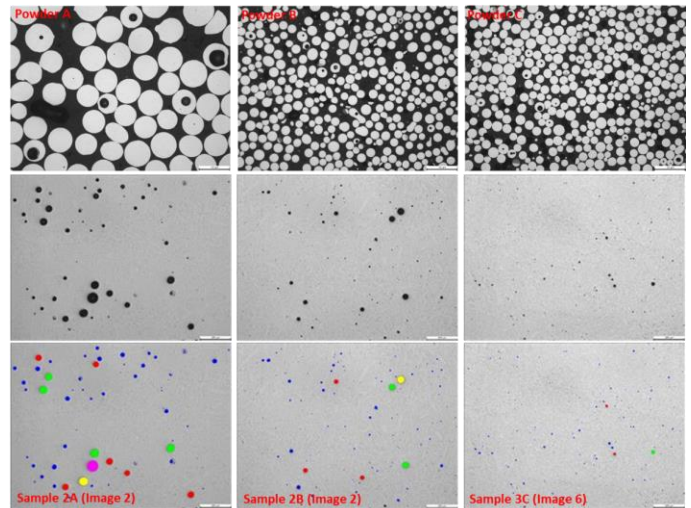

FIGURE 3: Example of internal porosity observed in the cross section (micrographs at 100X, polished) of powder particles in Alloy A, B and C (above). Rounded porosity observed with different LMD process parameters sets (center), and recognition of porosity after detection and classification in the image analysis, different colors represent different size range of the porosity detected (down).

The mean value and deviation of the calculated porosity percentage in six micrographs for each sample is compiled in the Table 3 and their evolution with the composition grade and LMD process parameters set is showed in the bars graph of Figure 4.

Table 3. Summary of porosity percentage calculated in powder particles and in LMD cylinders

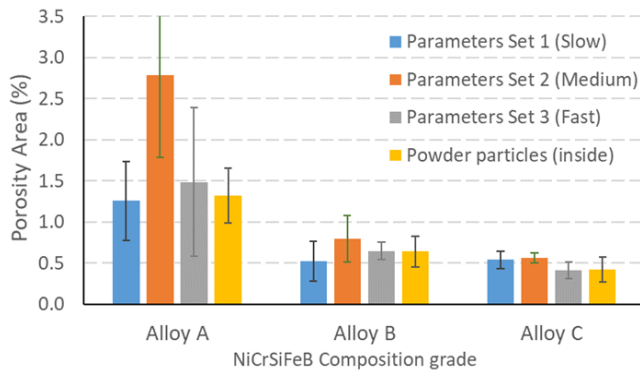| Condition	Porosity Area (%)		
	Alloy A	Alloy B	Alloy C
Powder Particles	1.32 ± 0.34	0.64 ± 0.19	0.43 ± 0.09
LMD parameters Set 1 (slow)	1.26 ± 0.48	0.53 ± 0.24	0.54 ± 0.11
LMD parameters Set 2 (medium)	2.78 ± 0.99	0.79 ± 0.28	0.57 ± 0.06
LMD parameters Set 3 (fast)	1.49 ± 0.90	0.65 ± 0.11	0.42 ± 0.10

FIGURE 4: Evolution of internal porosity evaluated in the cross section of powder particles and LMD cylinders of NiCrSiFeB alloys.

Optical examination was used to identify characteristic features of the material obtained by additive manufacturing by LMD. The layers located in the middle zone of each cylinder had a very fine microstructure but growing slightly on the slow process parameter used (set-1). The dendritic structure observed in the zones near to the cylinder´s surface and near to the build plate indicating that a very rapid cooling has taken place within the individual molten pool, after each laser track. The dendrite size for process parameter set-1 is the largest, decreasing for set-2 and set-3 according to the increase in the cooling speed and solidification rate (see Figure 5).
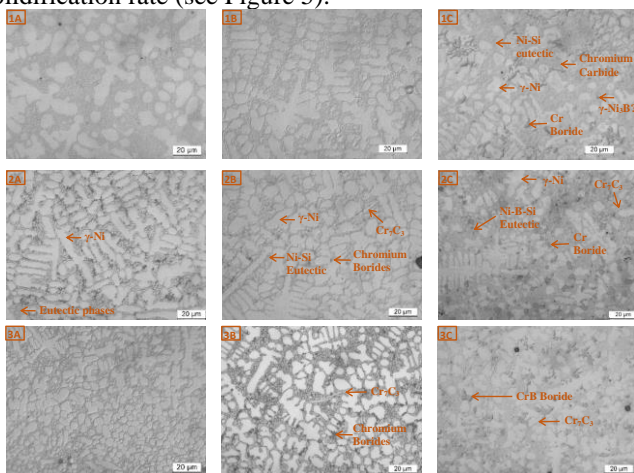

FIGURE 5: Micrographs (1000X, etched) for the different composition grades (A, B and C) obtained with different LMD process parameters set studied (1, 2 and 3)

The matrix phase is a solid solution of Ni with some Cr and Fe providing a dendritic structure (γ-Ni phase). There is an interdendritic lamellar eutectic phase made up mainly of Ni and small amounts of Si (Ni-Si Eutectics phase) according to the chemical composition obtained by EDS. Different shaped precipitates permeate the matrix (CrB and Ni_3B) but are mostly concentrated on the NiCrSiFeB composition grade C (Ni_3B, on Ni-B-Si eutectic phase). The precipitating of the carbides (Chromium carbides compound) is visible only at the grades B and C using optical microscopy. The analysis made in the LOM micrographs was supported by the identification of the phases/precipitates/segregates after a deep FESEM analysis with semi-quantitative measurements using EDS microanalysis and chemical composition maps. The main phases identified are showed in Figure 6 for composition grade C obtained with process parameter set 2 as example of the work done.
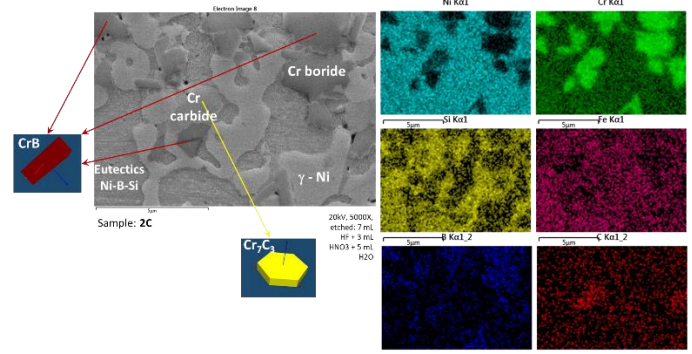

FIGURE 6: FESEM analysis and EDS maps of XZ plane for composition grade C and LMD process parameters set 2 (medium speed)

A comparative analysis of the hardness behaviour at room temperature and at high temperature were made. In the following graph (Figure 7) can be observed the mean values and deviation of the hardness values, evaluated in the nine NiCrSiFeB disc samples obtained by LMD, and in Stellite 6 as reference material. Hot hardness of alloy C is even higher than in Stellite 6 alloy.
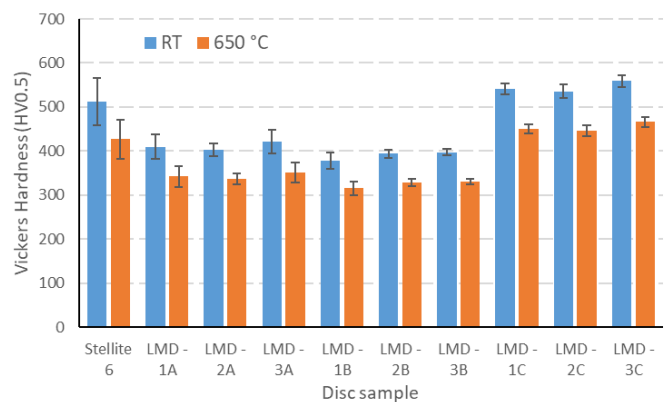

FIGURE 7: Vickers Hardness values in LMD samples and in Stellite 6, tested at RT (25 °C) and at HT (650 °C)

The only NiCrSiFeB composition grade that exceeds the RT and HT hardness of Stellite 6 is alloy C. In the microstructure of this alloy has been observed the presence of carbides and borides, enhancing the precipitation hardening mechanism, in

addition to potential solid solution hardening of the gamma Nickel matrix and the eutectic due the presence of Si and B. Borides are not present in alloy A and in very low quantity in alloy B.

Considering the good results achieved in terms of material processability, densification, microstructure, and hardness in as built condition (without heat treatment), in particular using the composition grade C, it seems feasible to plan a new fabrication route for the objective components, using the LMD process for the fabrication of the preform (near-net-shape) and following with non-destructive inspection, stress relieve HT, electric discharge machining (EDM) cutting, and machining and grinding to obtain the final part. In the following schema (Figure 8) is showed the new manufacturing route proposed.

FIGURE 8: New manufacturing route by laser metal deposition with the NiCrSiFeB alloy C proposed.

4. CONCLUSION

It is possible to process nickel-based self-fluxing alloys from the Ni-Cr-Si-B family with direct metal deposition using lasers. The alloy C deposited with the highest speed studied, has the highest densification and hardness in as-built condition (without heat-treatment), reaching 559 HV (54 HRC) at room temperature, which decreases to 466 HV (47 HRC) at high temperature (650 ℃). These values are higher than those of the Stellite 6 obtained by centrifugal casting, where 512 HV (50 HRC) and 427 HV (44 HRC) are reached respectively. Based on the promising results, a new manufacturing route using laser metal deposition is proposed. This study will be completed with tribological tests at high temperature in the three alloys studied, to evaluate the wear kinetics and the glaze layer formation, and a more advanced microstructural analysis to better understand the hardening mechanisms of NiCrSiFeB alloys processed by LMD and potential influence of the derived microstructure.

REFERENCES

[1] K. Simunovic, T. Saric, and G. Simunovic, "Different Approaches to the Investigation and Testing of the Ni-Based Self-Fluxing Alloy Coatings—A Review. Part 1: General Facts, Wear and Corrosion Investigations," *Tribol. Trans.*, vol. 57, no. 6, pp. 955–979, Nov. 2014, doi: 10.1080/10402004.2014.927547.

[2] K. Simunovic, S. Havrlisan, T. Saric, and D. Vukelic, "Modeling and Optimization in Investigating Thermally Sprayed Ni-Based Self-Fluxing Alloy Coatings: A Review," *Materials (Basel).*, vol. 13, no. 20, 2020, doi: 10.3390/ma13204584.

[3] J. Li, Y. Wang, Z. Lyu, N. Sharma, S. D. Choudhury, and L. Li, "Fracture of Ni-Cr-Si-B thermal sprayed and fused reciprocating pump rods during straightening," *Eng. Fail. Anal.*, vol. 127, p. 105576, 2021, doi: https://doi.org/10.1016/j.engfailanal.2021.105576.

[4] I. Hemmati, V. Ocelík, and J. T. M. De Hosson, "Effects of the Alloy Composition on Phase Constitution and Properties of Laser Deposited Ni-Cr-B-Si Coatings," *Phys. Procedia*, vol. 41, pp. 302–311, 2013, doi: https://doi.org/10.1016/j.phpro.2013.03.082.

[5] I. Hemmati, V. Ocelík, and J. T. M. De Hosson, "Dilution effects in laser cladding of Ni–Cr–B–Si–C hardfacing alloys," *Mater. Lett.*, vol. 84, pp. 69–72, 2012, doi: https://doi.org/10.1016/j.matlet.2012.06.054.

[6] L. Rong, D. Yinping, and K. Kafeel, "Advanced Super Alloys with High Performance for Severe Operation Environment Applications," *Int. J. Trend Res. Dev. (IJTRD). Proc. Int. Conf. Innov. Pract. Manag. Eng. Soc. Sci.*, pp. 8–14, 2019.

[7] International Organization for Standardization, "ISO/ASTM 52900:2015 Additive manufacturing — General principles — Terminology." ISO/TC 261 Additive manufacturing Technical Committee, Geneva, The Switzerland, 2015, [Online]. Available: https://www.iso.org/standard/69669.html.

[8] P. Aubry *et al.*, "Laser cladding of nickel base hardfacing material: Material analyses and manufacturing process evaluation on a scale one demonstrator," *J. Laser Appl.*, vol. 33, no. 1, p. 12005, 2021, doi: 10.2351/7.0000305.

[9] S. Qian, Y. Zhang, Y. Dai, and Y. Guo, "Microstructure and Mechanical Properties of Nickel-Based Coatings Fabricated through Laser Additive Manufacturing," *Metals (Basel).*, vol. 11, no. 1, 2021, doi: 10.3390/met11010053.